Mineralogy, Textures, and Relative Age Relationships of Massive Sulfide Ore in the West Shasta District, California

STEPHEN S. HOWE

U. S. Geological Survey, 345 Middlefield Road, Mail Stop 901, Menlo Park, California 94025

Abstract

The Devonian massive sulfide orebodies of the West Shasta district in northern California are composed primarily of pyrite, with lesser amounts of other sulfide and gangue minerals. Examination of polished thin sections of more than 100 samples from the Mammoth, Shasta King, Early Bird, Balaklala, Keystone, and Iron Mountain mines suggests that mineralization may be divided into six paragenetic stages, the last five each separated by an episode of deformation: (1) precipitation of fine-grained, locally colloform and framboidal pyrite and sphalerite; (2) deposition of fine-grained arsenopyrite and coarse-grained pyrite, the latter enclosing tiny inclusions of pyrrhotite; (3) penetration and replacement of sulfide minerals of stages 1 and 2 along growth zones and fractures by chalcopyrite, sphalerite, galena, tennantite, pyrrhotite, bornite, and idaite; (4) recrystallization and remobilization of existing minerals, locally increasing their size and euhedralism and promoting their aggregation; (5) deposition of quartz, white mica, chlorite, and calcite; and (6) formation of bornite, digenite, chalcocite, and covellite during supergene enrichment of several orebodies at the Iron Mountain mine. Despite regional greenschist facies metamorphism and local heating by intrusive bodies, enough of the original depositional features of the ore remain to suggest that the deposits in the district formed by processes similar to those that formed Kuroko- and Besshi-type massive sulfide deposits. Mineralogic and textural evidence do not support a second major episode of massive sulfide mineralization during the Permian.

Introduction

IN recent years, detailed studies by Barton (1978), Eldridge (1981), and Eldridge et al. (1983) of the mineralogy and textures of ore in the relatively pristine Kuroko-type massive sulfide deposits have resulted in a dramatic revision in the understanding of the paragenesis of these deposits. This modification has played an important role in the development of the most recent model for the formation of Kuroko-type deposits (cf. Ohmoto and Skinner, 1983). The success of these studies has stimulated a reexamination of ore minerals and textures in metamorphosed massive sulfide deposits, including Besshi-type deposits (Yui, 1983) and the more intensely deformed Appalachian deposits (Craig, 1983), in an attempt to unravel their depositional and metamorphic histories. As Craig (1983) points out, this challenge may be overwhelming in highly metamorphosed deposits containing sulfide minerals that reequilibrate readily. On the other hand, microscopic examination of deposits dominated by refractory sulfide minerals, such as pyrite and sphalerite, which have not been subjected to metamorphism above greenschist facies, should reveal a wealth of information. For this reason, a microscopic investigation of ore in the massive sulfide deposits of the West Shasta copper-zinc district in northern California was initiated as part of a broader study of the district (Albers, 1985).

The present paper describes and illustrates the mineralogy and textures of the ore in most of the major massive sulfide deposits in the district and incorporates these observations into a paragenetic sequence summarizing the relative age relationships of the sulfide and nonsulfide minerals. These features of the West Shasta ore are compared with those of Kuroko- and Besshi-type massive sulfide deposits, and the bearing of these characteristics on depositional processes is examined. Finally, recent K-Ar dating of the West Shasta ore by Kistler et al. (1985) is examined in light of the relative age relationships outlined here.

General Features of the West Shasta Orebodies and Ore

The geologic setting of the massive sulfide deposits in the West Shasta district is well described by Kinkel et al. (1956), Albers et al. (1981), Casey and Taylor (1982), Reed (1984), and Albers and Bain (1985) and is only briefly summarized here. The orebodies occur within the upper part of the middle unit of the Early Devonian Balaklala Rhyolite, on or near the axes of broad synclinal, and less commonly anticlinal, folds along a northeast-trending zone 13 km long by 3 km wide (Fig. 1). The largest deposits consist of massive, generally lenticular and flat-lying, pyritic bodies with lengths and widths commonly an order of magnitude greater than their thicknesses; contacts between these bodies and barren or weakly pyritized wall rocks are sharp. Stockworklike sulfide veins and disseminations
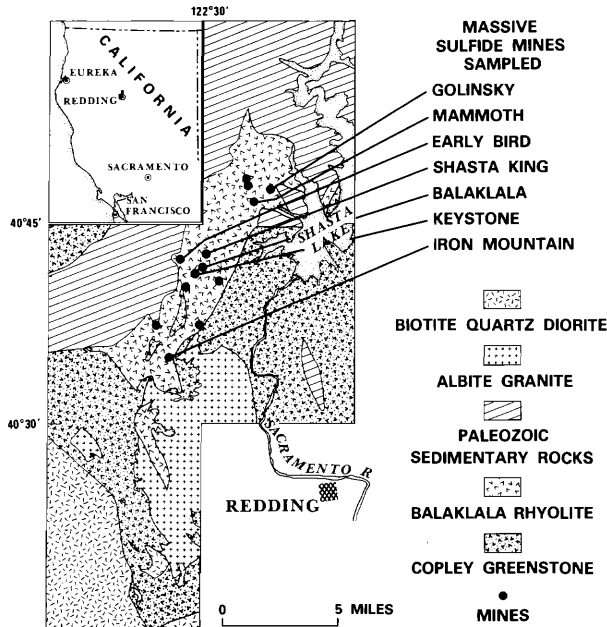
FIG. 1. Location map of principal mines and the generalized geologic setting of the West Shasta district. The Mule Mountain stock is shown here as albite granite and the Shasta Bally batholith as biotite quartz diorite.

occur locally beneath the massive lenses. The Balaklala Rhyolite is intruded by the Early Devonian Mule Mountain stock, which is itself intruded by the Late Jurassic Shasta Bally batholith. The district has undergone regional greenschist facies metamorphism.

The ore is composed mainly of massive pyrite with relatively minor amounts of chalcopyrite, sphalerite, galena, and quartz. Compositional layering is present locally. The ore has been deformed and recrystallized to varying degrees, compromising the preservation of original depositional textures and resulting in a somewhat chaotic mixture of breccia fragments, crystal aggregates, and minor crosscutting veins.

The ore grade ranges from 2.0 to 6.0 percent Cu and from 1.3 to 8.9 percent Zn. According to Kinkel et al. (1956), the lack of zinc assays at many of the mines prevents the determination of Cu/Zn ratios. Minor amounts of gold and silver have been recovered from the massive sulfide ore and from overlying gossan.

Mineralogy, Texture, and Paragenesis

Singly polished thick and thin sections, and doubly polished thin sections, of 137 samples from six mines in the district were examined (see Table 1) using reflected and transmitted light microscopes. A scanning electron microscope and an electron microprobe were not available during this study.

The mineralogy of the ore is relatively simple and consistent in all of the samples examined. The primary

sulfide minerals, in decreasing abundance, are pyrite, chalcopyrite, sphalerite, galena, tetrahedrite-tennantite (hereafter referred to as tennantite), arsenopyrite, pyrrhotite, bornite, idaite, and two unidentified phases. The nonsulfide minerals, in decreasing abundance, are quartz, white mica, calcite, chlorite, and iron oxides. Digenite, bornite, covellite, and chalcocite comprise the secondary sulfide minerals.

The growth habits, textures, and associations of the minerals comprising the ore are also broadly similar throughout the district, allowing the depositional and metamorphic histories of the deposits to be divided into six paragenetic stages (Fig. 2): (1) "primitive" pyrite + sphalerite; (2) pyrite ± arsenopyrite; (3) chalcopyrite + sphalerite + galena + tennantite + quartz + white mica; (4) recrystallization and remobilization; (5) quartz + white mica + calcite; and (6) supergene enrichment. These stages are described below.

Stage 1: "Primitive" pyrite + sphalerite

Mineralization in the West Shasta district appears to have begun with the precipitation of framboidal, colloform, and very fine grained pyrite, collectively termed "primitive" pyrite after Barton (1978). Framboids, a large proportion preserved as iron oxide pseudomorphs, have been observed in ore from the Mammoth mine where they reach a maximum diameter of 25 μm. Colloform pyrite occurs in ore from the Mammoth and Keystone mines as aggregates of curvilinear bands up to 2 mm in length (Fig. 3A) or as individual spheroids 15 to 90 μm in diameter. Some spheroids have been selectively replaced by chalcopyrite, sphalerite, and galena along concentric growth zones (Fig. 3B) whereas other spheroids have been completely replaced, leaving circular voids entirely filled by later sulfides (termed here "bullet hole texture") (Fig. 3C). Porous and pitted aggregates up to 4 mm in diameter of very fine grained (<10 μm) subhedral to euhedral pyrite crystals constitute the most abundant and widespread primitive pyrite.

Similar aggregates of fine-grained sphalerite, up to 4 mm in diameter and locally porous and pitted, also appear to be early formed or primitive. The temporal relationship between primitive pyrite and sphalerite is not clear, but both phases predate stage 2.

TABLE 1. Location and Number of Samples Examined

Mine	Number
Mammoth	10
Shasta King	2
Early Bird	2
Balaklala	9
Keystone	1
Iron Mountain	113

STAGE	1	2	3	4	5	6

MINERAL
  PYRITE
  ARSENOPYRITE
  PYRRHOTITE
  BORNITE, IDAITE
  CHALCOPYRITE
  SPHALERITE
  GALENA
  TENNANTITE
  UNKNOWN B
  QUARTZ
  WHITE MICA
  CHLORITE
  CALCITE
  DIGENITE
  CHALCOCITE
  COVELLITE
  IRON OXIDES
DEFORMATION
  BRECCIATION
  FRACTURING
  RECRYST., REMOB.
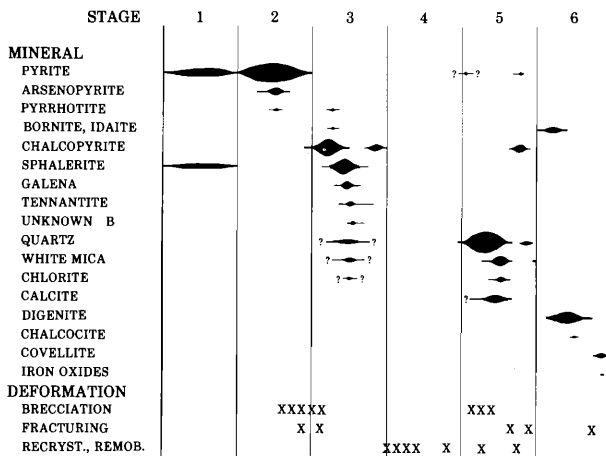
FIG. 2. Generalized paragenesis of the massive sulfide mineralization in the West Shasta district. Bar thickness indicates relative abundance of the mineral. Number of x's indicates relative intensity of the deformational episode. Question marks indicate uncertainty in the duration of mineral precipitation.

Stage 2: Pyrite ± arsenopyrite

The deposition of the primitive sulfides was followed by the main episode of pyrite precipitation during stage 2. Subhedral to euhedral crystals of pyrite, mostly cubes and pyritohedrons < 1 μm to 2 mm in diameter, were deposited during stage 2. Where not recrystallized, pyrite occurs mainly as dense disseminations and in loosely packed clusters of randomly oriented crystals and crystal fragments (Fig. 3D). The clusters locally surround clasts of primitive pyrite. Several pyrite crystals completely enclose a few small, isolated pyrrhotite subhedra.

Euhedral, rhombic to wedge-shaped crystals of arsenopyrite, up to 80 μm in length but generally much shorter, are sparsely intergrown with stage 2 pyrite.

Stage 2 mineralization was followed by an episode of district-wide deformation, the severity of which ranged from moderate fracturing (Fig. 3D) to intense brecciation and shearing (Fig. 3E and F) that occurred during at least two separate events (Fig. 3F).

Stage 3: Chalcopyrite + sphalerite + galena + tennantite + quartz + white mica

Precipitation of base metal sulfides and replacement of stage 2 pyrite occurred in three episodes during stage 3. During the earliest episode, chalcopyrite was deposited along fractures in pyrite and between breccia fragments. In some samples, particularly those from the Iron Mountain mine, fractures have been filled without appreciable replacement of the host, resulting in matching walls of pyrite on each side of the fracture. In other samples, however, fractures are enlarged by replacement of the pyrite by chalcopyrite (Fig. 3G). Some pyrite fragments show

selective replacement of cores and growth zones by chalcopyrite (Fig. 3H), whereas other fragments are extensively embayed (Fig. 4A). Chalcopyrite also forms gashlike veins and fills V-shaped voids in aggregates of primitive pyrite and sphalerite from the Mammoth mine during this episode of stage 3. At the Mammoth and Shasta King mines, chalcopyrite replaces arsenopyrite euhedra formed in stage 2 (Fig. 4B).

Minute, rounded, oval inclusions and thin stringers of pyrrhotite, bornite, idaite, and an unidentified bluish-gray mineral ("unknown A") with optical properties somewhat similar to rutite and hematite, completely enclosed by pyrite, appear to have been deposited toward the end of the early episode of stage 3. Pyrrhotite and bornite in separate stringers both replace pyrite and are in contact locally with chalcopyrite and sphalerite (Fig. 4C). Idaite, in contact with bornite, was identified in two rounded inclusions < 5 μm in diameter.

Sphalerite was deposited during the middle episode of stage 3. Although it is neither as abundant nor as widespread as chalcopyrite, it comprises the majority of the banded ore from the Friday-Louden portal at the Mammoth mine and is locally the most abundant sulfide in some samples from the Mammoth, Shasta King, and Iron Mountain mines. Kinkel et al. (1956) noted that the Yolo and Graton orebodies at the Mammoth mine were particularly zinc rich. Sphalerite exhibits many of the same textures and associations shown by chalcopyrite deposited during the earliest episode of stage 3. Like chalcopyrite, sphalerite penetrates pyrite and replaces it along fractures. Sphalerite generally fills the more proximal portions of fractures occupied by both sphalerite and chalcopyrite, suggesting that sphalerite postdates chalcopyrite deposited during the earliest episode of stage 3. Sphalerite also selectively replaces cores (Fig. 4D) and growth zones in some pyrite fragments and embays the margins of other fragments (Fig. 4E).

Galena and tennantite were both deposited during the middle episode of stage 3, but their positions in the paragenetic sequence are not firmly established owing to their minor abundance in the ore. Both minerals penetrate and replace stage 2 pyrite along fractures which locally contain chalcopyrite distally (Fig. 4F). At the Iron Mountain mine, galena penetrates shears in previously brecciated pyrite fragments. Tennantite replaces arsenopyrite euhedra at the Mammoth and Shasta King mines (Fig. 4B). Galena and tennantite commonly are intergrown with one another and with chalcopyrite and sphalerite. Locally chalcopyrite embays galena but is itself replaced by tennantite, suggesting that tennantite postdates galena slightly. Both galena and tennantite vein stage 3 sphalerite at the Iron Mountain mine. Dense clusters of submicron-sized needles and blebs of tennantite in

stage 3 sphalerite (Fig. 4G) form patches that are reddish-brown in transmitted light and resemble patches in Kuruko ores observed by Barton (1978).

In one sample from the Iron Mountain mine, an unidentified brownish-gray mineral ("unknown B") with optical properties somewhat similar to enargite occurs as rounded inclusions < 10 μm in diameter in tennantite in contact with sphalerite. The unidentified phase exsolves from or replaces sphalerite but has a mutual boundary texture with tennantite.

Quartz, white mica, and chlorite were also deposited during stage 3, probably during the middle episode. Unfractured euhedral quartz is surrounded by chalcopyrite and tennantite in several samples from the Iron Mountain mine. Locally the quartz margins are embayed by tennantite.

The last episode of stage 3 is characterized by chalcopyrite replacement of sphalerite in a manner resembling the chalcopyrite disease of Barton (1978). Irregular, rounded, or lathlike blebs of chalcopyrite, all < 5 μm, occur as fine dustings, trains, or myrmekitic forms (Fig. 4H) concentrated along crystal boundaries and minute fractures. Locally chalcopyrite-diseased sphalerite embays larger masses of chalcopyrite that were deposited during the early episode of stage 3. The younger chalcopyrite has no apparent spatial relationship to the older chalcopyrite.

Stage 4: Recrystallization and remobilization

Stage 4 is characterized not by deposition of new minerals but by recrystallization and remobilization of existing minerals. Harder, more brittle sulfide minerals such as pyrite and sphalerite are recrystallized while softer, more malleable minerals such as chalcopyrite, galena, and tennantite are remobilized.

Recrystallization promoted the aggregation of pyrite fragments that had been fractured at the end of stage 2 and penetrated and replaced by chalcopyrite, sphalerite, galena, and tennantite during stage 3 (Fig. 5A). Recrystallization also increased the size and euhedralism of stage 2 pyrite, most dramatically for crystals that are disseminated or in loosely packed clusters surrounded by chalcopyrite, galena, or void space (Fig. 5B). Recrystallization of more tightly packed, nearly monomineralic aggregates of pyrite resulted in local interpenetrations of fragments and the development of triple junctions among fragments (Fig. 5C). Irregular inclusions and fracture fillings of stage 3 sulfide minerals and quartz in pyrite have been annealed locally; all that remain are rounded to myrmekitic blebs concentrated in the cores of the pyrite crystals (Fig. 5C and D).

Recrystallization also resulted in sphalerite aggregates that contain crystals or fragments which have been previously replaced by chalcopyrite. Although recrystallization increased the size of the chalcopyrite blebs, the original orientation of rows of chalcopyrite

inclusions and chalcopyrite along fractures have been preserved. These markers are oriented in a different direction for nearly each of the individual sphalerite fragments comprising the aggregates, indicating that the fragments coalesced in a crystallographically random fashion. Original color banding in sphalerite has largely been obliterated in aggregates by the homogenizing influence of recrystallization. Only in sphalerite that has been shielded from the effects of recrystallization by surrounding sulfide masses has color banding been preserved (Fig. 5E).

Originally fine-grained white mica and chlorite in the groundmass of sparsely mineralized host rocks apparently increased in size and locally acquired a preferred orientation during stage 4. Stage 3 white mica also increased in size during stage 4, seemingly at the expense of sphalerite and, less commonly, pyrite and chalcopyrite (Figs. 4E and 5F), suggested by the enclosure of fragments of the sulfide minerals by the white mica. The crystals are usually scattered without discernible orientation within the recrystallized sulfide minerals (see fig. 8 in Craig, 1983), but in ore from the Friday-Louden portal of the Mammoth mine, white mica flakes in sphalerite are subparallel to megascopic compositional layering (Fig. 5G).

A minor amount of stage 3 chalcopyrite has been remobilized into previously unfilled fractures in stage 2 pyrite and into pressure shadows during stage 4. Chalcopyrite derived from stage 3 also replaces the margins of recrystallized pyrite euhedra that contain blebs of tennantite annealed during stage 4 (Fig. 5D).

Stage 5: Quartz + white mica + calcite

Pyrite was the first mineral deposited during stage 5. Euhedral crystals locally coat previously recrystallized pyrite aggregates and project into vugs filled later by quartz.

A major episode of quartz precipitation followed pyrite deposition. Quartz penetrates and replaces stage 2 pyrite along fractures that were not filled by stage 3 sulfide minerals (Fig. 5H). It surrounds pyrite aggregates, locally embaying the margins of the recrystallized pyrite. Quartz veins frequently enclose fragments of stage 2 pyrite that are crosscut and replaced by stage 3 sulfide minerals (Fig. 6A), indicating that the quartz postdates stage 3. Two samples from the Iron Mountain mine have textures suggesting that the quartz not only postdates stage 3 but also the recrystallization during stage 4. In one sample, quartz surrounds pyrite euhedra that in turn enclose rounded chalcopyrite blebs (Fig. 6B). In the other sample, a 25-μm-wide fracture filled by deformed quartz cuts across a pyrite aggregate in which the cores of the pyrite crystals comprising the aggregate are replaced by rounded inclusions of chalcopyrite and sphalerite. Quartz deposited during stage 5 shows a variety of deformation textures. Most common is the develop-

ment of polycrystalline quartz with undulatory extinction. Slightly increased deformation resulted in the suturing of contacts between crystallites through pressure solution and a mottling of crystallites (and their extinctions) by the nucleation of submicron-sized protocrystallites. In rare instances, the intensity of the deformation produced a cataclastic texture. One of the more common textures of the quartz (first noted by Kinkel et al., 1956) is a subparallel arrangement of lathlike crystallites with slightly sutured contacts, termed here "feather quartz." In places it lines vein walls, surrounding more equant polycrystalline quartz in the interior of the veins. Elsewhere, it completely fills veins where the optical continuity of the individual crystallites is not interrupted by pyrite fragments in the center of the veins. Feather quartz also surrounds individual crystals or fragments of pyrite and pyrite aggregates, the laths usually oriented with their long axes at right angles to the margin of the pyrite (Fig. 6C). Often the quartz feathers completely surround the pyrite, but locally they develop only on opposite sides of the pyrite or near corners of the pyrite crystals or fragments. In samples where both relict quartz phenocrysts and pyrite crystals or fragments are surrounded by a groundmass of fine-grained quartz, white mica, and chlorite, quartz laths extend only from the margins of the pyrite (Fig. 6D). Late fractures locally cut across deformed quartz, intersecting the submicron-sized protocrystallites and larger crystallite boundaries; they are marked by trains of secondary two-phase fluid inclusions. The fractures also offset gashlike veins and pods filled with deformed feather quartz (Fig. 6E).

White mica and lesser amounts of chlorite were deposited with quartz. As deformation and recrystallization of the quartz intensified, flakes of white mica and chlorite recrystallized along the elongate quartz crystallite contacts. In several samples, feather quartz and intergranular white mica are both deformed, locally with distinct kinking.

Calcite fills large voids and fractures in a sample from the Early Bird mine (Fig. 6F) but has not been recognized elsewhere in the district. The calcite encloses fragments of pyrite replaced by chalcopyrite-diseased sphalerite and surrounds euhedral pyrite with cores replaced by rounded sphalerite blebs. The calcite exhibits prominent deformation lamellae and is cut locally by late fractures.

Recrystallization and remobilization during stage 5 resulted in the deposition of pyrite euhedra and massive chalcopyrite around the margins of voids in older pyrite and quartz aggregates, and the deposition of chalcopyrite in fractures and along grain boundaries in polycrystalline quartz (Fig. 6G). As the abundance of this stage 5 chalcopyrite is quite significant locally, some of it may have been newly precipitated rather than just remobilized from existing masses. Hairline,

locally horsetailing, fractures commonly cut stage 5 chalcopyrite.

At the end of stage 5, undeformed quartz filled the voids lined by stage 5 chalcopyrite. Trace amounts of white mica fill hairline fractures that cut both feather and unstrained quartz.

Stage 6: Supergene enrichment

This stage includes oxidation and supergene enrichment of the ore. Oxidation is widespread but very insignificant. Iron oxides, associated in places with covellite, locally penetrate horsetailing hairline fractures that cut the ore and sparsely mineralized host rocks.

Supergene enrichment of the ore by formation of copper sulfide minerals occurred in the Brick Flat, Mattie, and Old Mine orebodies at the Iron Mountain mine but is most advanced in the Old Mine orebody. Bornite, the first stage 6 mineral to form, occurs as irregular masses locally embaying pyrite and is completely surrounded by digenite. Locally bornite encloses submicron-sized inclusions of chalcopyrite. Digenite veins and partly replaces chalcopyrite and bornite (Fig. 6H). It surrounds, but does not replace, rounded pyrite fragments that were partly replaced by stage 3 chalcopyrite. Minor amounts of chalcocite have mutual boundary textures with digenite that is associated with chalcopyrite and bornite. Covellite replaces chalcopyrite, sphalerite, and tennantite along late hairline fractures in samples from the Brick Flat and Mattie orebodies, but it is most abundant at the Old Mine orebody. It also penetrates hairline fractures in dignite and chalcocite. Covellite locally surrounds pyrite fragments that have been previously replaced by chalcopyrite; the covellite does not replace the pyrite but attacks the chalcopyrite entensively.

Depositional and Metamorphic Histories of the Deposits

The paragenetic sequence outlined in this paper summarizes the relative age relationships of the sulfide and nonsulfide minerals in most of the major deposits in the West Shasta district. Due to the regional greenschist facies metamorphism and local heating by a variety of plutons, the depositional histories of the deposits are somewhat obscured by metamorphic events. However, a careful study of the ore allows the unraveling of portions of both the depositional and metamorphic histories of the deposits.

The mineralogy of the West Shasta ores is nearly identical to that of ores in Kuroko-type deposits, although their proportions are somewhat different (Shimazaki, 1974; Eldridge et al., 1983). More striking is the similarity of mineral textures in the West Shasta ores to those exhibited by Kuroko- and Besshi-type deposits (see especially figs. 10 A–H, 11 A–H, and 23a in Eldridge et al., 1983; figs. 4, 5, 6 in Ko-

muro, 1984; and figs. 10–12, 14, 15, and 17a–h in Yui, 1983). For the Kuroko ores, the particularly good geologic control, the recognition of several distinct ore types (e.g., tetsusekiei, massive black ore, powdery yellow ore, and siliceous black ore), and the preservation of primary depositional features allow an especially detailed paragenesis to be constructed. The use of the term "facies" rather than "stage" in the paragenetic sequence in Eldridge et al. (1983) reflects the high quality of the data on spatial relationships in the Kuroko ores. Such stringent constraints on the paragenesis of the mineralization in the West Shasta district are not possible, but a comparison of the paragenesis of the ores in the West Shasta and Hokuroko districts reveals a number of similarities. These include early precipitation of fine-grained and colloform (primitive) pyrite and sphalerite, renewed precipitation and coarsening of pyrite and other iron sulfide minerals, replacement of earlier formed sulfides by later base metal sulfides, and deposition of quartz toward the end of the sequence. These similarities in the mineralogy, textures, and paragenesis among the West Shasta, Kuroko, and Besshi ores suggest that all three were formed by similar depositional processes.

It is uncertain whether recrystallization and remobilization in the West Shasta deposits during stage 4 (and continuing during portions of stage 5) were caused by temperature increases and dissolution within the accumulating sulfide sediment, by local heating around plutons intruded after most of the mineralization was completed, by greenschist facies metamorphism, or by some combination of these events. However, the bulk of the quartz, white mica, and chlorite formed during stage 5, definitely post-dating main ore deposition. Kistler et al. (1985) report K-Ar ages of about 370 m.y. for most of the samples of sericite from the massive ore in the Brick Flat orebody at the Iron Mountain mine, 30 m.y. younger than the Balaklala Rhyolite. However, a few samples from the Brick Flat orebody yielded K-Ar ages of 290 to 252 m.y., leading them to suggest a second episode of mineralization, possibly related to the emplacement of the Pit River stock dated at about 261 m.y. (J. P. Albers, oral commun., 1985) east of the West Shasta district. The minor amounts of pyrite and chalcopyrite deposited with quartz and white mica at the end of stage 5 indicate that this later event was probably not a second episode of massive sulfide mineralization but

rather a recrystallization and remobilization of earlier minerals (and partial resetting of the older K-Ar ages) due to heating by the Pit River stock.

Acknowledgments

REFERENCES

Albers, J. P., 1985, An issue devoted to the West Shasta massive deposits—Introduction: ECON. GEOL., v. 80, p. 2067–2071.

Albers, J. P., and Bain, J. H. C., 1985, Regional setting and new information on some critical geologic features of the West Shasta district, California: ECON. GEOL., v. 80, p. 2072–2091.

Albers, J. P., Kistler, R. W., and Kwak, L., 1981, The Mule Mountain stock, an early Middle Devonian pluton in northern California: Isochron/West, no. 31, p. 17.

Barton, P. B., Jr., 1978, Some ore textures involving sphalerite from the Furutobe mine, Akita Prefecture, Japan: Mining Geology, v. 28, p. 293–300.

Casey, W. H., and Taylor, B. E., 1982, Oxygen, hydrogen, and sulfur isotope geochemistry of a portion of the West Shasta Cu-Zn district, California: ECON. GEOL., v. 77, p. 38–49.

Craig, J. R., 1983, Metamorphic features in Appalachian massive sulphides: Mineralog. Magazine, v. 47, p. 515–525.

Eldridge, C. S., 1981, Mineral textures and parageneses of Kuroko ores from the Uwamuki No. 4 and some other Kuroko deposits, Hokuroku district, Japan: Unpub. M.S. thesis, The Pennsylvania State Univ., 104 p.

Eldridge, C. S., Barton, P. B., Jr., and Ohmoto, H., 1983, Mineral textures and their bearing on formation of the Kuroko orebodies: ECON. GEOL. MON. 5, p. 241–281.

Kinkel, A. R., Jr., Hall, W. E., and Albers, J. P., 1956, Geology and base-metal deposits of the West Shasta copper-zinc district, Shasta County, California: U. S. Geol. Survey Prof. Paper 285, 156 p.

Kistler, R. W., McKee, E. H., Futa, K., Peterman, Z. E., and Zartman, R. E., 1985, A reconnaissance Rb-Sr, Sm-Nd, U-Pb, and K-Ar study of some host rocks and ore minerals in the West Shasta Cu-Zn district, California: ECON. GEOL., v. 80, p. 2128–2135.

Komuro, K., 1984, Textures of the Kuroko ores from the Ezuri mine, Akita Prefecture: Mining Geology, v. 34, p. 251–262.

Ohmoto, H., and Skinner, B. J., eds., 1983, The Kuroko and related volcanogenic massive sulfide deposits: ECON. GEOL. MON. 5, 604 p.

Reed, M. H., 1984, Geology, wall-rock alteration, and massive sulfide mineralization in a portion of the West Shasta district, California: ECON. GEOL., v. 79, p. 1299–1318.

Shimazaki, Y., 1974, Ore minerals of the Kuroko-type deposits: Mining Geology Spec. Issue 6, p. 311–322.

Yui, S., 1983, Textures of some Japanese Besshi-type ores and their implications for Kuroko deposits: ECON. GEOL. MON. 5, p. 231–240.

Photomicrographs of the West Shasta Mineralization

Figures 3 through 6 were taken in reflected light unless indicated otherwise. The abbreviations for the minerals are as follows: ap = arsenopyrite, bn = bornite, ca = calcite, cp = chalcopyrite, cv = covellite, dg = digenite, gn = galena, po = pyrrhotite, py = pyrite, qz = quartz, sp = sphalerite, tn = tennantite, wm = white mica.

FIG. 3. A.   Aggregate of curvilinear bands of stage 1 colloform pyrite selectively replaced by stage 3 chalcopyrite. G4, Keystone mine. Scale bar = 52 μm. B. Spheroids of stage 1 colloform pyrite selectively replaced by stage 3 chalcopyrite and sphalerite along concentric growth zones. FL1, Mammoth mine. Scale bar = 104 μm. C. Complete replacement of spheroids of stage 1 colloform pyrite; the resulting circular voids are entirely filled by stage 3 chalcopyrite (bullet hole texture). G4, Keystone mine. Scale bar = 52 μm. D. Fractured stage 2 pyrite crystals. Note nearly perfectly matching walls of pyrite fragments, left center. Stage 5 quartz surrounds the pyrite fragments. 661, Iron Mountain mine. Scale bar = 104 μm. E. Intensely brecciated stage 2 pyrite showing a wide range in fragment sizes. The larger masses are aggregates of smaller fragments. Stage 5 quartz surrounds the fragments. IM-28, Iron Mountain mine. Scale bar = 207 μm. F. Rebrecciation of stage 2 pyrite fragments. Note shearing of large fragment in the center of the photograph and presence of many smaller pyrite fragments between the two pieces of the large fragment. Stage 5 quartz surrounds the pyrite fragments. IM-5, Iron Mountain mine. Scale bar = 52 μm. G. Fractured stage 2 pyrite replaced by stage 3 chalcopyrite. Note late fracture running from the top to the bottom of the photograph, cutting both the pyrite and the chalcopyrite. G2, Mammoth mine. Scale bar = 104 μm. H. Stage 3 chalcopyrite and very minor stage 3 galena and sphalerite have selectively replaced stage 2 pyrite along concentric growth zones. IM-26, Iron Mountain mine. Scale bar = 52 μm.
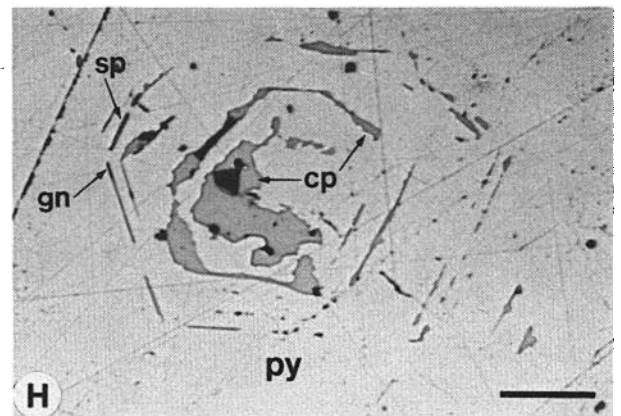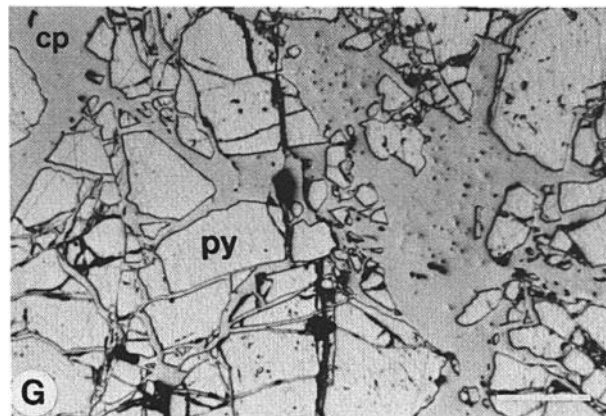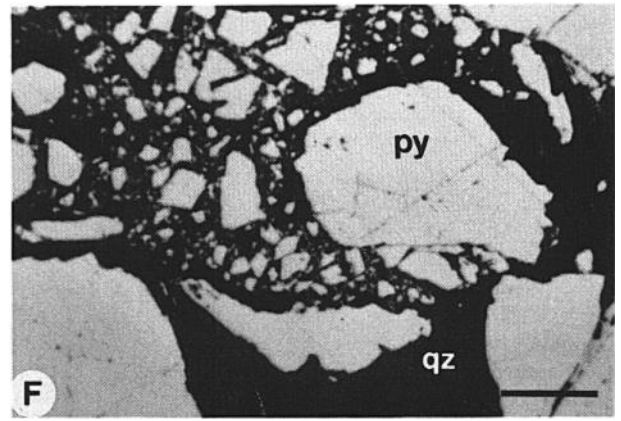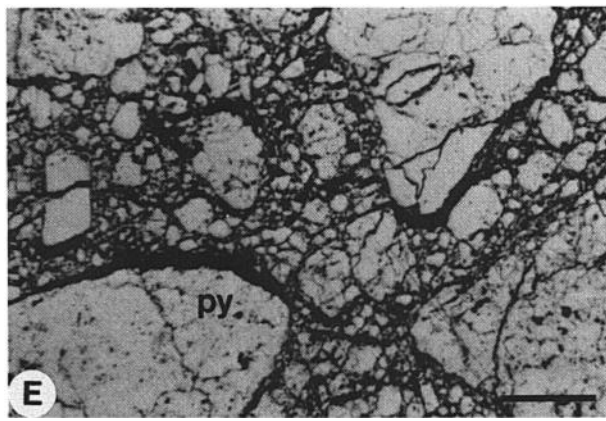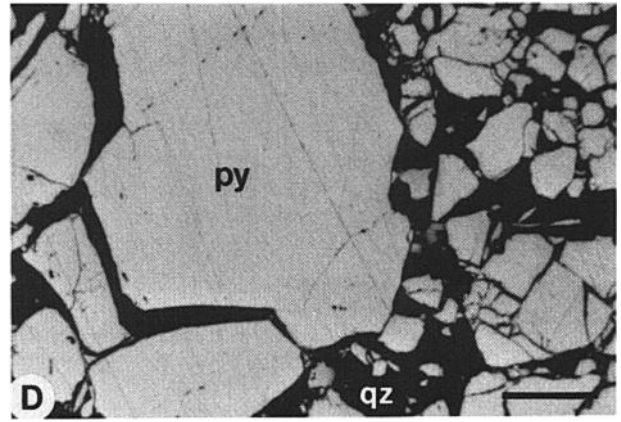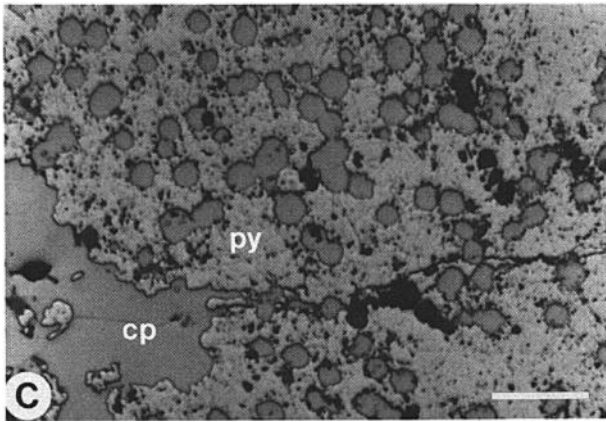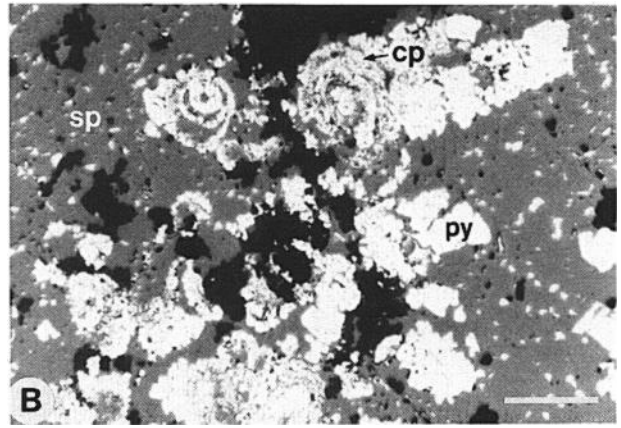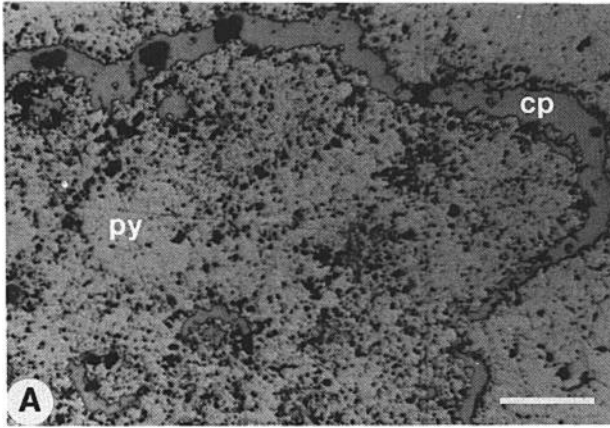
FIG. 4. A. Subhedral stage 2 pyrite extensively embayed by stage 3 chalcopyrite, tennantite, and sphalerite. 658, Iron Mountain mine. Scale bar = 52 μm. B. Rhombic to wedge-shaped crystals of stage 2 arsenopyrite replaced by stage 3 chalcopyrite, tennantite, and galena. Note the scalloped margins of the arsenopyrite euhedra in contact with chalcopyrite. Tennantite appears to have replaced selectively the arsenopyrite along growth zones. 671, Mammoth mine. Scale bar = 52 μm. C. Stringers of stage 3 pyrrhotite, in contact with stage 3 sphalerite, have replaced stage 2 pyrite. IM-46, Iron Mountain mine. Scale bar = 21 μm. D. Stage 3 sphalerite has selectively replaced the core of subhedral stage 2 pyrite. Stage 5 quartz surrounds the pyrite. IM-37, Iron Mountain mine. Scale bar = 52 μm. E. Stage 3 sphalerite embaying margins of stage 2 pyrite subhedra. Flakes of stage 3 white mica are enclosed within sphalerite. 658, Iron Mountain mine. Scale bar = 52 μm. F. Stage 3 tennantite and chalcopyrite have penetrated and replaced stage 2 pyrite along fractures. Stage 3 galena not visible in this photograph. IM-19, Iron Mountain mine. Scale bar = 21 μm. G. Submicron-sized needles and blebs of stage 3 tennantite in stage 3 sphalerite. IM-23, Iron Mountain mine. Scale bar = 21 μm. H. Tiny lathlike blebs of late stage 3 chalcopyrite have replaced middle stage 3 sphalerite in the center of the photograph. More massive early stage 3 chalcopyrite has replaced stage 2 pyrite subhedra around the margins of the field but is itself embayed by the sphalerite. IM-19, Iron Mountain mine. Scale bar = 21 μm.
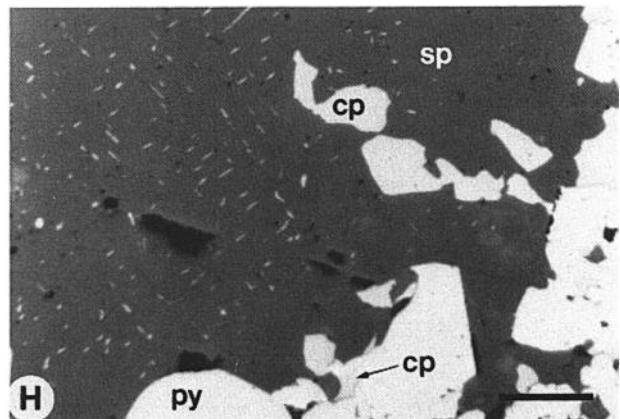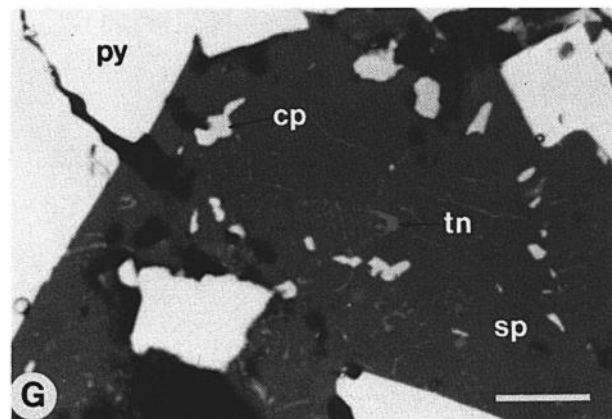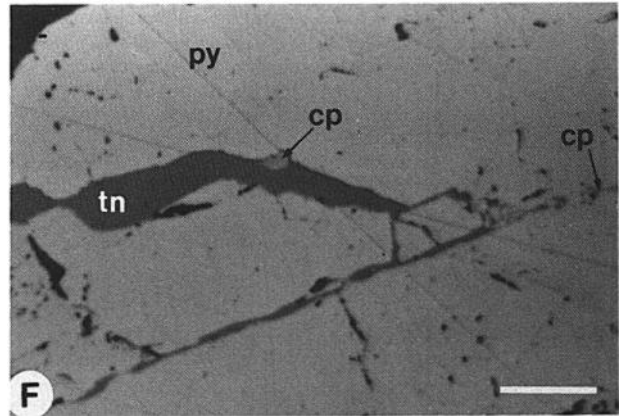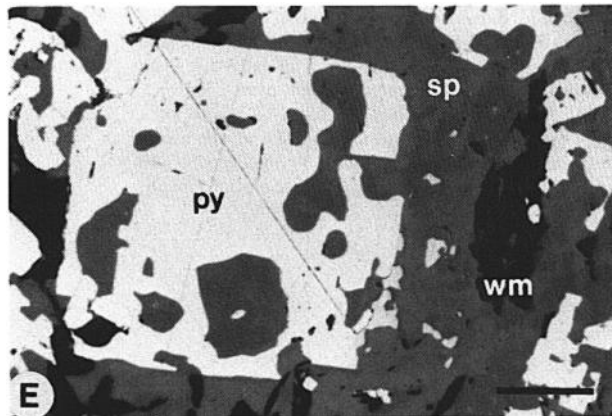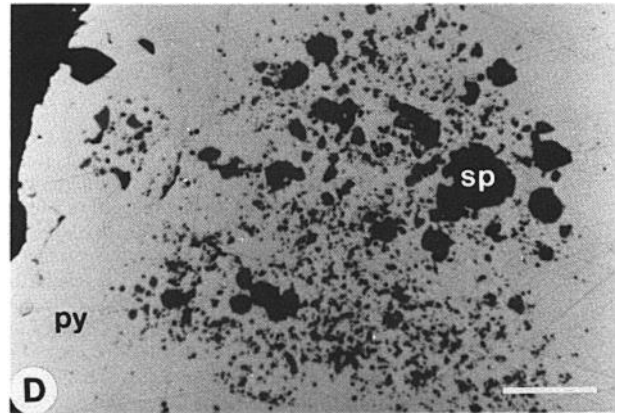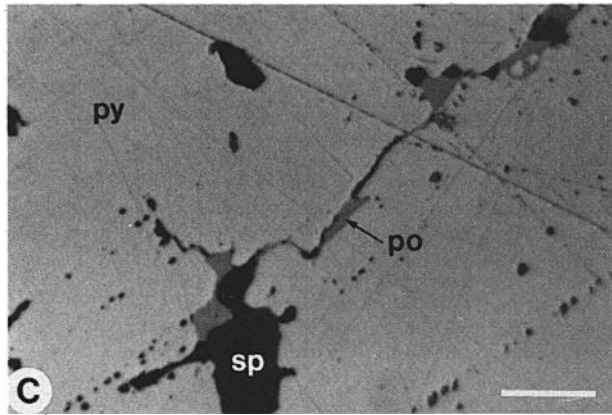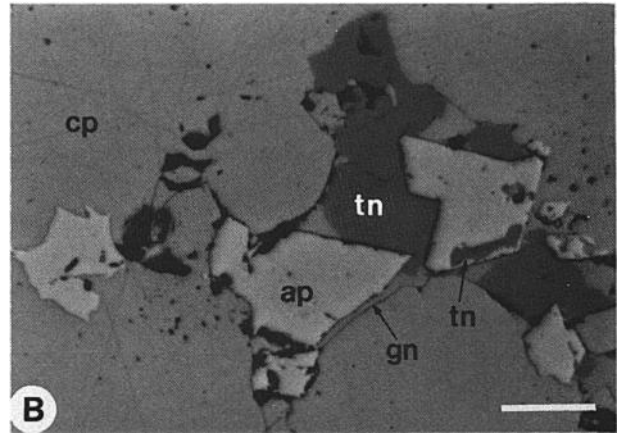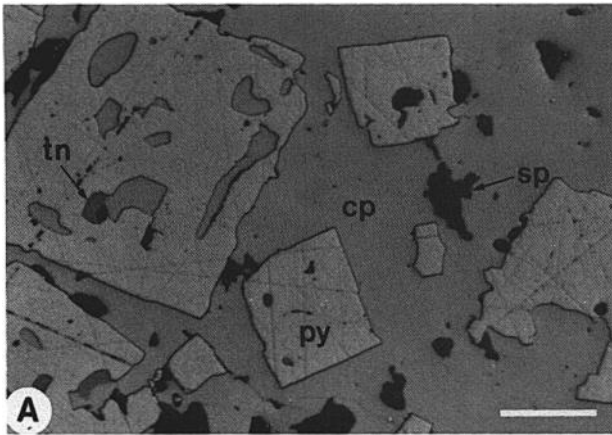
FIG. 5. A.   Partial aggregation of stage 2 pyrite fragments containing irregular stage 3 chalcopyrite
and sphalerite inclusions resulting from recrystallization in stage 4. Stage 5 quartz surrounds aggregates.
IM-8, Iron Mountain mine. Scale bar = 52 μm. B. Aggregates of stage 2 pyrite fragments partly replaced
by stage 3 chalcopyrite. Recrystallization increased most dramatically the size and euhedralism of
crystals projecting into voids which were later filled by stage 5 quartz. Note the rounded nature of the
chalcopyrite inclusions in the pyrite crystals. IM-38, Iron Mountain mine. Scale bar = 52 μm. C.
Rounded to myrmekitic blebs of stage 3 sphalerite concentrated in the cores of stage 2 pyrite fragments
in recrystallized aggregates. Note obliteration of pyrite fragment margins, interpenetration of fragments,
and the formation of triple junctions among fragments. IM-15, Iron Mountain mine. Scale bar = 21
μm. D. Rounded to myrmekitic blebs of stage 3 tennantite concentrated in the core of a recrystallized
stage 2 pyrite crystal. The crystal originally projected into a void which has been filled by stage 5
quartz. Note replacement of the pyrite and intersection of the annealed tennantite blebs by stage 3
chalcopyrite which was remobilized during stage 4. IM-26, Iron Mountain mine. Scale bar = 21 μm.
E. Stage 3 sphalerite filling bullet hole voids in stage 1 colloform pyrite. Reddish-brown color banding
is preserved in the outer margin. G4, Keystone mine. Transmitted light. Scale bar = 52 μm. F. Laths
of stage 3 white mica apparently replacing stage 3 chalcopyrite. Note projection of laths into the
chalcopyrite and the fragments of chalcopyrite enclosed by the white mica. Minor pyrite, galena,
tennantite, and sphalerite also present. IM-26, Iron Mountain mine. Scale bar = 52 μm. G. White mica
flakes in stage 3 sphalerite subparallel to megascopic compositional layering. FL1, Mammoth mine.
Scale bar = 104 μm. H. Fractured stage 2 pyrite penetrated and replaced by stage 3 chalcopyrite and
stage 5 quartz. Note offset of one of the chalcopyrite-filled fractures in the center of the photograph.
IM-5, Iron Mountain mine. Scale bar = 52 μm.
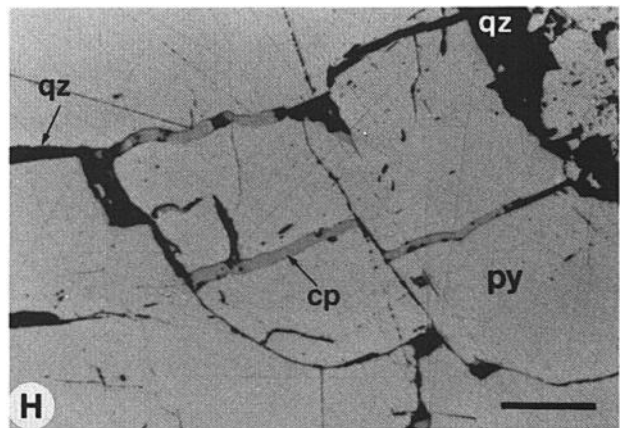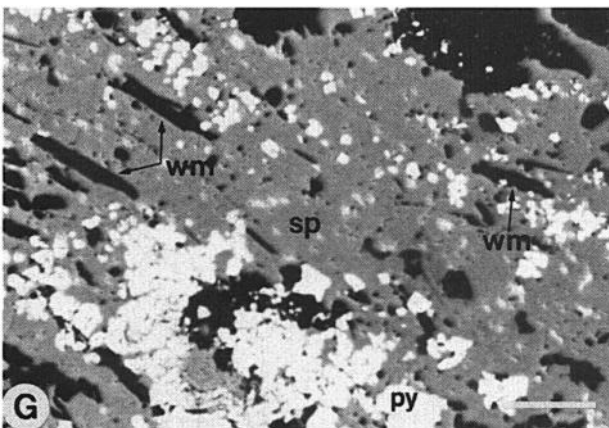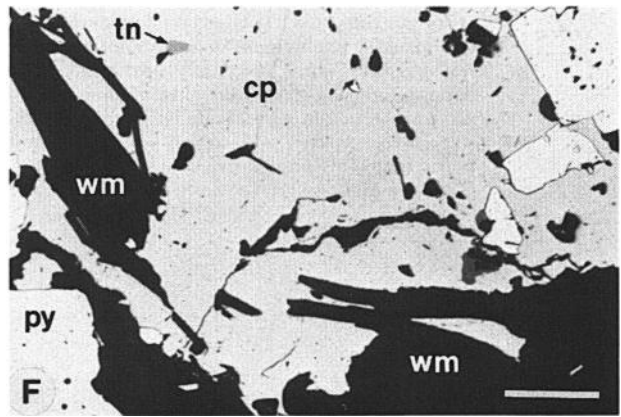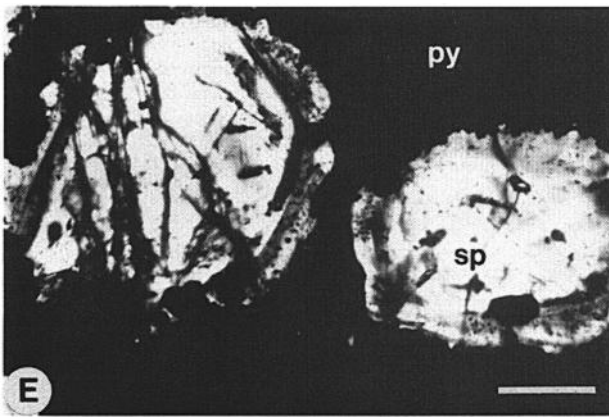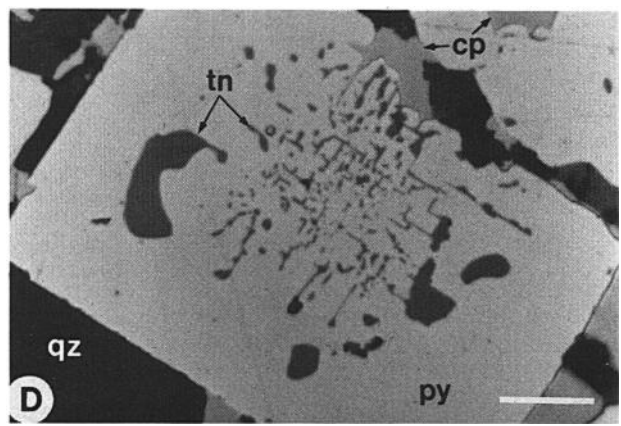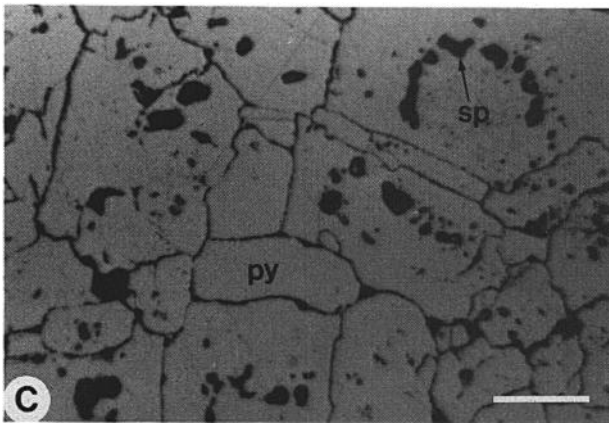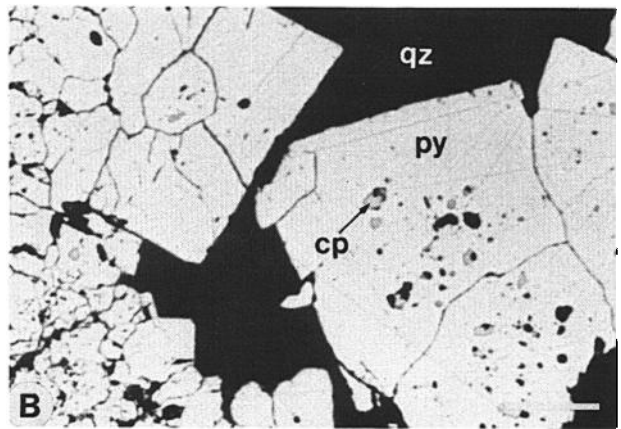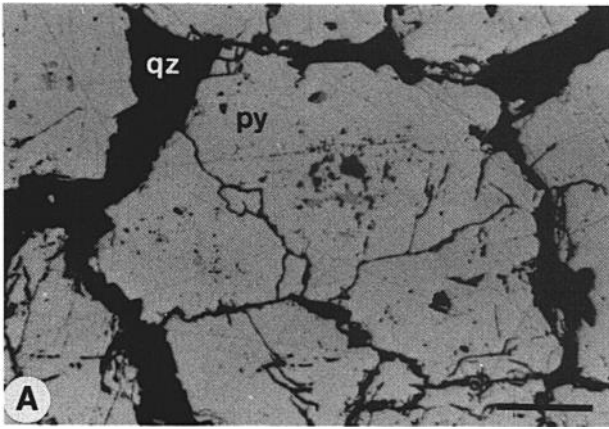
FIG. 6. A.   Stage 5 quartz vein enclosing fragments of stage 2 pyrite. These fragments are penetrated and replaced by stage 3 sulfide minerals elsewhere in the sample. A late fracture, not clearly visible in this photograph, cuts the quartz vein. IM-23, Iron Mountain mine. Scale bar = 207 μm. B. Stage 5 quartz surrounds recrystallized stage 2 pyrite euhedra that in turn enclose rounded blebs of stage 3 chalcopyrite. IM-13, Iron Mountain mine. Scale bar = 52 μm. C. Lathlike crystallites of stage 5 feather quartz with their long axes subperpendicular to the margin of a stage 2 pyrite crystal. Stage 5 white mica is intergrown with and locally replaces the quartz. IM-46, Iron Mountain mine. Transmitted light, crossed polars. Scale bar = 132 μm. D. Stage 5 feather quartz extending from margins of stage 2 pyrite crystals whereas margins of relict quartz phenocrysts are barren of feather quartz. IM-42A, Iron Mountain mine. Transmitted light, crossed polars. Scale bar = 334 μm. E. Late fractures offset gashlike veins and pods filled with deformed feather quartz in aggregate of fine-grained brecciated stage 2 pyrite. IM-9, Iron Mountain mine. Scale bar = 207 μm. F. Stage 5 calcite fills void into which projects a large recrystallized stage 2 pyrite crystal, penetrating the pyrite along fractures running from the top to the bottom of the photograph. Deformation lamellae in calcite not visible in photograph. Stage 3 chalcopyrite replaces the pyrite. 566, Early Bird mine. Scale bar = 104 μm. G. Massive and vein chalcopyrite deposited during stage 5 in voids, fractures, and along grain boundaries in polycrystalline quartz. IM-25, Iron Mountain mine. Scale bar = 207 μm. H. Anastamosing veinlets of stage 6 digenite replacing stage 3 chalcopyrite and stage 6 bornite. Digenite surrounds, but does not replace, rounded stage 2 pyrite fragments previously corroded by chalcopyrite. Trace amounts of stage 6 covellite also present. 651, Iron Mountain mine. Scale bar = 52 μm.